Inorg. Chem. **2006**, *45*, 6227–6234

On the Disorder of the Cl Atom Position in and Its Probable Effect on the Magnetic Properties of $(CuCl)LaNb_2O_7$

Myung-Hwan Whangbo* and Dadi Dai

Department of Chemistry, North Carolina State University, Raleigh, North Carolina 27695-8204

Received January 18, 2006

The magnetic susceptibility of $(CuCl)LaNb_2O_7$ shows a spin gap despite the Cu^{2+} ions in each $CuClO_2$ layer forming a square lattice. To account for this observation, we explored implications of the disorder of the Cl-atom position in $(CuCl)LaNb_2O_7$ by considering possible ordered structures of $CuCl_4O_2$ octahedra in each $CuClO_2$ layer, by identifying various spin exchange interactions of a $CuClO_2$ layer and by estimating the relative strengths of these interactions in terms of spin dimer analysis. We then probed what kind of spin lattice is required for each $CuClO_2$ layer to have a spin gap on the basis of the classical spin approximation. Our study suggests that the $CuCl_4O_2$ octahedra of each $CuClO_2$ layer should be arranged such that the resulting spin lattice does not have uniform chains but ring clusters containing an even number of Cu atoms. Implications of this conclusion were discussed on the basis of the recently reported neutron scattering and magnetization studies of $(CuCl)LaNb_2O_7$.

1. Introduction

The crystal structure[1] of $(CuCl)LaNb_2O_7$ is made up of CuCl sheets (Figure 1a) and Nb_2O_7 double-perovskite slabs (Figure 1b), with the La^{3+} ions located at the 12-coordinate sites of the double-perovskite slabs. The CuCl sheets alternate with the Nb_2O_7 slabs along the *c* direction such that each $CuCl_4$ square of a CuCl sheet is axially capped by two oxygen atoms to form a $CuCl_4O_2$ octahedron (Figure 1c), and every CuCl sheet becomes a $CuClO_2$ layer (Figure 1d). The Cu^{2+} ions of the $CuClO_2$ layers are the only magnetic ions of $(CuCl)LaNb_2O_7$ and form a square lattice. The X-ray powder diffraction study[1] of $(CuCl)LaNb_2O_7$ reported that the Cl atoms in each CuCl sheet are located at the centers of the Cu_4 squares, so that each $CuCl_4O_2$ octahedron has D_{4h} symmetry with Cu−Cl = 2.746 Å and Cu−O = 1.841 Å. The Cu−Cl bond is rather long compared with the value expected from the ionic radii sum (i.e., 2.54 Å).[2] This coordinate environment (i.e., four long and two short bonds) is unusual for a Cu^{2+} ion. A realistic picture for the coordinate environment of the Cu^{2+} ions was provided by the neutron powder diffraction study,[3] which shows that the Cl atom in each Cu_4 square is displaced from its center to the four split positions around it (Figure 2a). By selecting one of the four split positions for each Cl, every $CuCl_4O_2$ octahedron can have two short Cu−Cl (hereafter referred to as $Cu-Cl_s$) and two long Cu−Cl (hereafter referred to as $Cu-Cl_l$) bonds (i.e., 2.402 and 3.142 Å, respectively).

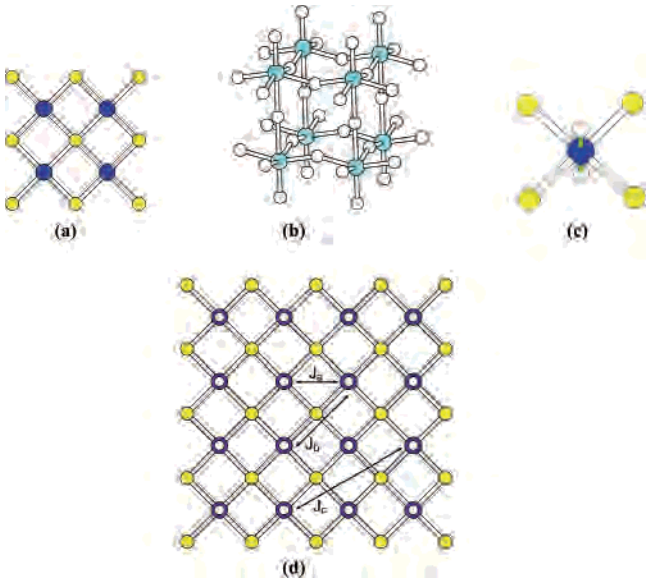

Figure 1. Structural building blocks of $(CuCl)LaNb_2O_7$: (a) CuCl sheet, (b) Nb_2O_7 slab, (c) $CuCl_4O_2$ octahedron, and (d) $CuClO_2$ layer. The blue, yellow, cyan, and white circles represent the Cu, Cl, Nb, and O atoms, respectively.

* To whom correspondence should be addressed. E-mail: mike_whangbo@ncsu.edu.

(1) Kodenkandath, T. A.; Lalena, J. N.; Zhou, W. L.; Carpenter, E. E.; Sangregorio, C.; Falster, A. U.; Simmons, W. B., Jr.; O'Connor, C. J.; Wiley: J. B. *J. Am. Chem. Soc.* **1999**, *121*, 10743.
(2) Shannon, R. D. *Acta Crystallogr. A* **1976**, *32*, 751.
(3) Caruntu, G.; Kodenkandath, T. A.; Wiley: J. B. *Mater. Res. Bull.* **2002**, *37*, 593.

10.1021/ic060104w CCC: $33.50
Published on Web 07/11/2006

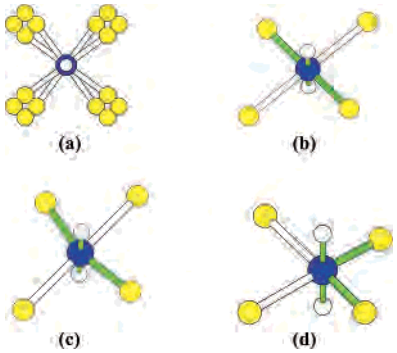

Figure 2. Structures of $CuCl_4O_2$ octahedra: (a) undistorted $CuCl_4O_2$ octahedron with four split positions for each Cl, (b) distorted $CuCl_4O_2$ octahedron with linear $Cl_s-Cu-Cl_s$, (c) distorted $CuCl_4O_2$ octahedron with slightly bent $Cl_s-Cu-Cl_s$, and (d) distorted $CuCl_4O_2$ octahedron with $\angle Cl_s-Cu-Cl_s = 90°$. In (b)−(d) the four bonds around the Cu atom are shown as green cylinders.

Consequently, the resulting octahedron has four short (i.e., two Cu−O and two Cu−Cl_s) and two long (i.e., two Cu−Cl_l) bonds, which is the usual coordinate environment for a Cu^{2+} ion. An example is shown in Figure 2b, where the two Cu−O and two Cu−Cl_s bonds form a $CuCl_2O_2$ rhombus with linear $Cl_s-Cu-Cl_s$. The disorder of the Cl-atom position means that, in the $CuClO_2$ layers of $(CuCl)LaNb_2O_7$, the $CuCl_4O_2$ octahedra with two short and two long Cu−Cl bonds are present without long-range order in their orientation and shape (see below).

When its $CuClO_2$ layers are considered to form a square spin lattice, the magnetic properties of $(CuCl)LaNb_2O_7$ are quite puzzling to understand.[4,5] If the $CuCl_4O_2$ octahedra of $(CuCl)LaNb_2O_7$ possess D_{4h} symmetry as suggested by the X-ray powder diffraction study, each $CuClO_2$ layer forms a square spin lattice defined by two spin exchange interactions J_a and J_b (Figure 1d).[1,4,5] In general, the spin exchange J_b through the linear Cu−Cl−Cu bridge should be more strongly antiferromagnetic than the spin exchange J_a through the Cu−Cl−Cu bridges with $\angle Cu-Cl-Cu = 90°$.[6] Thus, the spin lattice of the $CuClO_2$ layer is essentially a square spin lattice (defined by the spin exchange interactions J_b), the magnetic susceptibility of which is expected to have a broad maximum with nonzero value at $T = 0$.[7,8] Although the magnetic susceptibility of $(CuCl)LaNb_2O_7$ shows a broad maximum at 16.5 K,[1,4] it decreases sharply to zero below 16.5 K, hence leading to a spin gap (i.e., the energy gap that separates the singlet ground state from the first excited state). Surprisingly, the general features of the magnetic susceptibility of $(CuCl)LaNb_2O_7$ are reasonably well described by an isolated spin dimer model.[4] Furthermore, when an isolated spin dimer model is used to analyze the *Q*-dependence of the neutron scattering intensity profile measured for powder samples,[4] it is found that the Cu···Cu distance of the dimer is close to that of the fourth nearest-neighbor spin exchange interaction J_c (Figure 1d).

In view of the fact that the Cl-atom position in $(CuCl)LaNb_2O_7$ is disordered,[3] one should question if a square spin lattice is a proper model for $(CuCl)LaNb_2O_7$. In interpreting the magnetic properties of a magnetic compound, it is essential to identify its spin lattice (i.e., the lattice made up of strongly interacting spin exchange paths). It is frequently assumed that the spin lattice of a magnetic system containing transition metal ions with unpaired spins is the same as the geometrical arrangement of its metal ions. For a complex magnetic system, a spin lattice suggested by this intuitive appeal is often incorrect because the strength of a spin exchange interaction between two spin sites is not determined by the distance between the two spin sites but by the overlap between their magnetic orbitals.[9] Consequently, it is crucial to identify the spin lattice of a magnetic system on the basis of appropriate electronic structure calculations. So far, there has been no study concerning how the disorder of the Cl-atom position in $(CuCl)LaNb_2O_7$ might affect its spin exchange interactions and hence the topology of its spin lattice. The present work probes this and its related questions.

Our work is organized as follows. In Section 2, we search for a spin lattice model relevant for the $CuClO_2$ layer by examining the consequence of the disorder of the Cl-atom position on the coordinate environment of the Cu^{2+} ions in the $CuClO_2$ layer, identifying various spin exchange paths of the $CuClO_2$ layer, and then evaluating their relative strengths on the basis of spin dimer analysis. In Section 3, we discuss how one might use the classical spin approximation to predict whether a spin lattice has a spin gap and then probe what kind of spin lattice is required for the $CuClO_2$ layer to have a spin gap. Essential findings of our work are summarized in Section 4.

2. Spin Exchange Paths and Spin Dimer Analysis

2.1. Octahedral Distortion and Spin Exchange Paths. When all the $CuCl_4O_2$ octahedra have the four-short-two-long coordination (Figure 2b) with linear $Cl_s-Cu-Cl_s$ units, the $CuClO_2$ layer is divided into $CuClO_2$ chains of corner-sharing $CuCl_2O_2$ rhombuses (Figure 3). Because there are four different ways of selecting two short and two long Cu−Cl bonds for each $CuCl_4O_2$ octahedron, there occur four different $CuClO_2$ chain arrangements, as shown in Figure 3. If a $CuCl_4O_2$ octahedron is allowed to have a nonlinear $Cl_s-Cu-Cl_s$ unit, other types of Cu^{2+}-ion environments are possible. The $CuCl_4O_2$ octahedron of Figure 2c differs from that of Figure 2b since the $Cl_s-Cu-Cl_s$ unit is slightly bent ($\angle Cl_s-Cu-Cl_s = 162.1°$), but that of Figure 2d is considerably different with $\angle Cl_s-Cu-Cl_s = 90°$. When $CuCl_4O_2$ octahedra with nonlinear $Cl_s-Cu-Cl_s$ units are included, the $CuClO_2$ layers of $(CuCl)LaNb_2O_7$ can be divided into "ring clusters" containing an even number of Cu atoms (hereafter

(4) Kageyama, H.; Kitano, T.; Oba, N.; Nishi, M.; Nagai, S.; Hirota, K.; Viciu, L.; Wiley: J. B.; Yasuda, J.; Baba, Y.; Ajiro, Y.; Yoshimura, K. *J. Phys. Soc. Jpn.* **2005**, *74*, 1702.
(5) Kageyama, H.; Yasuda, J.; Kitano, T.; Totsuda, K.; Narumi, Y.; Hagiwara, M.; Kindo, K.; Baba, Y.; Oba, N.; Ajiro, Y.; Yoshimura, K. *J. Phys. Soc. Jpn.* **2005**, *74*, 3155.
(6) Goodenough, J. B. *Magnetism and the Chemical Bond*; Wiley: Cambridge, MA; 1963.
(7) Takahashi, M. *Phys. Rev. B* **1989**, *40*, 2494.
(8) Manousakis, E., *Rev. Mod. Phys.* **1991**, *63*, 1.
(9) For recent reviews, see: (a) Whangbo, M.-H.; Koo, H.-J.; Dai, D. *J. Solid State Chem.* **2003**, *176*, 417. (b) Whangbo, M.-H.; Dai, D.; Koo, H.-J. *Solid State Sci.* **2005**, *7*, 827.

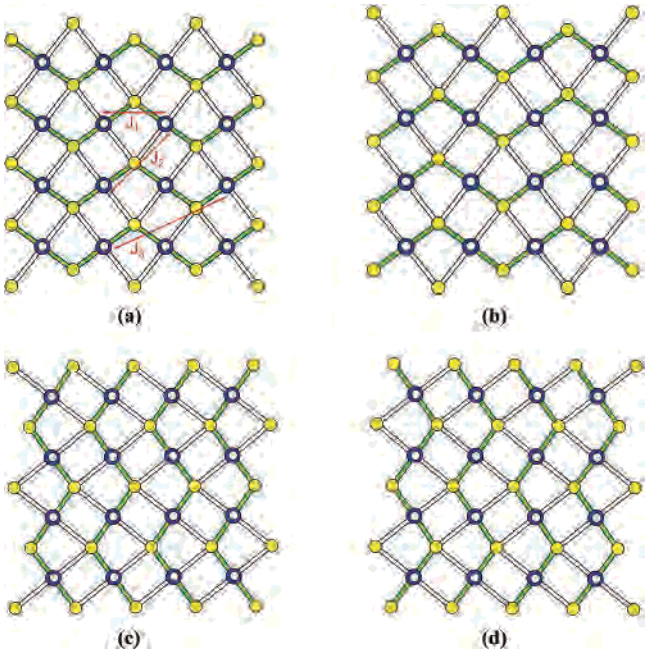

Figure 3. Four different arrangements of the $CuClO_2$ chains of a $CuClO_2$ layer that result when all the $CuCl_4O_2$ octahedra have the four-short-two-long coordination with linear $Cl_s-Cu-Cl_s$ units.

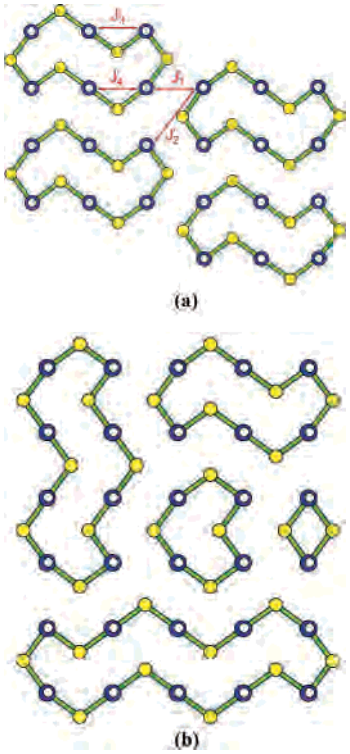

Figure 4. $CuClO_2$ layers composed of 2*n*-ring clusters: (a) a $CuClO_2$ layer with long-range order and (b) a $CuClO_2$ layer without long range order. For simplicity, the long Cu−Cl bonds are not shown.

referred to as 2*n*-ring clusters), as illustrated in Figure 4. In principle, each $CuClO_2$ layer can be divided into 2*n*-ring clusters of varying sizes with or without long-range order. However, it is likely that each $CuClO_2$ layer consists of 2*n*-ring clusters of similar size without long range order. In a ring cluster with $2n \geq 6$, each ring consists of two parallel chain fragments containing *n* Cu^{2+} ions, the two ends of which are each capped by a Cl_s atom.

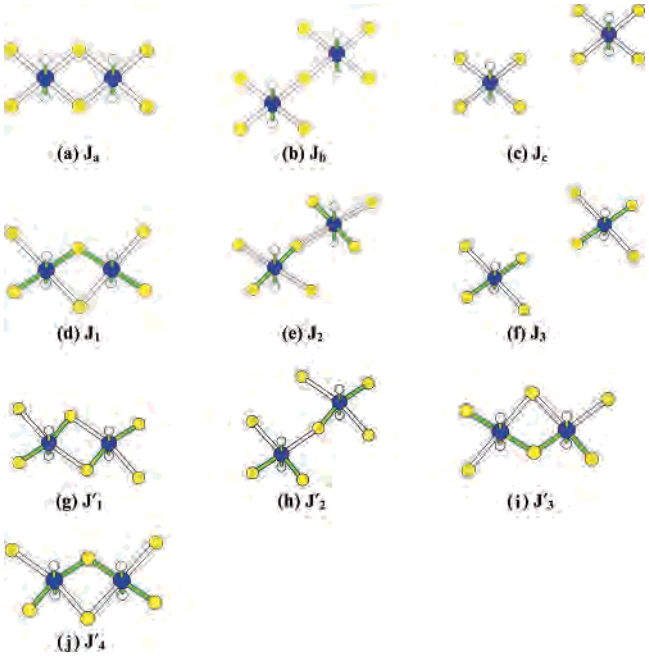

Figure 5. Spin dimers associated with the spin exchange interactions J_a, J_b, and J_c of the undistorted $CuClO_2$ layer (Figure 1d), J_1, J_2, and J_3 of the $CuClO_2$ layer composed of $CuClO_2$ chains (Figure 3a), and J'_1 J'_2, J'_3, and J'_4 of the $CuClO_2$ layer composed of 2*n*-ring clusters (Figure 4a).

The spin exchange interactions of interest for the "undistorted" $CuClO_2$ layer (Figure 1d) are J_a, J_b, and J_c. The spin dimers associated with these interactions are shown in Figure 5a−c. The corresponding spin exchange interactions in the "distorted" $CuClO_2$ layer consisting of $CuClO_2$ chains (Figure 3a) are J_1, J_2, and J_3. The spin dimers representing these interactions are shown in Figure 5d−f. For the $CuClO_2$ layers composed of 2*n*-ring clusters, there occur a number of different spin exchange paths within and between adjacent clusters, as shown by the interactions J'_1, J'_2, J'_3, and J'_4 in Figure 4a. The spin dimers representing these interactions are shown in Figure 5g−j. Some structural parameters associated with these spin exchange paths are summarized in Table 1.

2.2. Spin Dimer Analysis and Spin Lattice. The $CuCl_4O_2$ octahedra of Figures 1c, 2b, and 2d have the magnetic orbitals shown in Figures 6a, 6b, and 6c, respectively. For a spin dimer consisting of two spin sites, the two magnetic orbitals interact to give rise to an energy split Δe. When the two spin sites of a spin dimer are nonequivalent, their magnetic orbitals are different in energy by Δe^0. Obviously, $\Delta e^0 = 0$ if the two spin sites are equivalent. In the spin dimer analysis based on extended Hückel tight binding (EHTB) calculations, the strength of an antiferromagnetic interaction between two spin sites is estimated by considering the antiferromagnetic spin exchange parameter J_{AF},[9]

$$J_{AF} = -\frac{(\Delta\epsilon)^2}{U_{eff}} \qquad (1)$$

where $(\Delta\epsilon)^2 = (\Delta e)^2 - (\Delta e^0)^2$, and U_{eff} is the effective on-site repulsion that is essentially a constant for a given compound. Therefore, the trend in the J_{AF} values is deter-

Table 1. Geometrical Parameters and $(\Delta\epsilon)^2$ Values Associated with the Spin Exchange Interactions in the $CuClO_2$ Layers of $(CuCl)LaNb_2O_7$

undistorted $CuClO_2$ layer (Figure 1d)

	geometrical parameters[a]	$(\Delta\epsilon)^2$ [a]	
J_a	Cu···Cu = 3.884 Å Cu−Cl = 2.746 Å (×4) ∠Cu−Cl−Cu = 90° (×2)	8100	(0.23)
J_b	Cu···Cu = 5.492 Å Cu−Cl = 2.746 Å (×2) ∠Cu−Cl −Cu = 180°	35 000	(1.00)
J_c	Cu···Cu = 8.684 Å Cu−Cl = 2.746 Å (×2) Cl···Cl = 3.884 Å ∠Cu−Cl···Cl = 135.02° (×2)	820	(0.02)

$CuClO_2$ layer composed of $CuClO_2$ chains (Figure 3a)

	geometrical parameters[a]	$(\Delta\epsilon)^2$	
J_1	Cu···Cu = 3.884 Å Cu−Cl = 2.402 Å (×2) ∠Cu−Cl−Cu = 107.9°	25 000	(1.00)
J_2	Cu···Cu = 5.492 Å Cu−Cl = 2.402 Å, Cu···Cl = 3.142 Å ∠Cu−Cl···Cu = 164.2°	350	(0.01)
J_3	Cu···Cu = 8.684 Å Cu−Cl = 2.402 Å (×2) Cl···Cl = 4.025 Å ∠Cu−Cl···Cl = 159.2° (×2)	11 700	(0.47)

$CuClO_2$ layer with 2*n*-ring clusters (Figure 4a)

	geometrical parameters[a]	$(\Delta\epsilon)^2$	
J'_1	Cu···Cu = 3.884 Å Cu−Cl = 2.402 Å, Cu···Cl = 3.142 Å ∠Cu−Cl···Cu = 87.9°	150	(0.00)
J'_2	Cu···Cu = 5.492 Å Cu−Cl = 2.402 Å, Cu···Cl = 3.142 Å ∠Cu−Cl···Cu = 164.2°	25 000	(0.44)
J'_3	Cu···Cu = 3.884 Å Cu−Cl = 2.402 Å (×2) ∠Cu−Cl−Cu = 107.9°	56 700	(1.00)
J'_4	Cu···Cu = 3.884 Å Cu−Cl = 2.402 Å (×2) ∠Cu−Cl−Cu = 107.9°	29 000	(0.51)

[a] In units of $(meV)^2$. The numbers in the parentheses give the relative tendency for antiferromagnetic coupling.

mined by that in the corresponding $(\Delta\epsilon)^2$ values. The magnetic properties of a variety of magnetic solids are well described by the $(\Delta\epsilon)^2$ values obtained from EHTB calculations,[9] when both the d orbitals of the transition metal and the s/p orbitals of its surrounding ligands are represented by double-ζ Slater-type orbitals.[10] The atomic parameters used for the present EHTB calculations are summarized in Table 2. In this section, we examine the relative strengths of the various spin exchange interactions defined in Figures 1d, 3a, and 4a. The $(\Delta\epsilon)^2$ values calculated for these spin exchange interactions are summarized in Table 1.[11]

For the undistorted $CuClO_2$ layer (Figure 1d), Table 1 shows that the SE interaction J_b is the strongest antiferromagnetic spin exchange interaction. This interaction is strong due to the linear Cu−Cl−Cu bridge. The SSE interaction J_c is negligible because the small ∠Cu−Cl···Cl angle (135.0°) does not allow good overlap between the magnetic orbitals of the two spin sites (see below). The SE interaction J_a is weaker than J_b by a factor of about four. As expected, the undistorted $CuClO_2$ layer forms a square spin lattice defined by the interactions J_b with spin frustration from the interactions J_a.

Table 2. Exponents, ζ_i, and Valence Shell Ionization Potentials, H_{ii}, of Slater-type Orbitals, χ_i, Used for Extended Hückel Tight-Binding Calculation[a]

atom	χ_i	H_{ii} (eV)	ζ_i	C^b	ζ'_i	C'^b
Cu	4s	−11.4	2.151	1.0		
Cu	4p	−6.06	1.370	1.0		
Cu	3d	−14.0	7.025	0.4473	3.004	0.6978
Cl	3s	−26.3	2.927	0.6262	1.854	0.5051
Cl	3p	−14.2	2.624	0.5540	1.475	0.5519
O	2s	−32.3	2.688	0.7076	1.675	0.3745
O	2p	−14.8	3.694	0.3322	1.659	0.7448

[a] The diagonal matrix element H_{ii} is defined as $<\chi_i|H^{eff}|\chi_i>$, where H^{eff} is the effective Hamiltonian. In our calculations of the off-diagonal matrix elements $H^{eff} = <\chi_i|H^{eff}|\chi_j>$, the weighted formula was used. [b] Contraction coefficients used in the double-ζ Slater-type orbital.

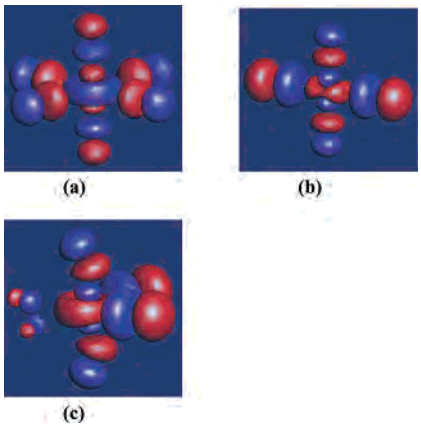

Figure 6. Magnetic orbitals for the $CuCl_4O_2$ octahedron of (a) Figure 1c, (b) Figure 2b, and (c) Figure 2d.

For the $CuClO_2$ layer composed of $CuClO_2$ chains (Figure 3), Table 1 shows that the SE interaction J_1 is the strongest antiferromagnetic spin exchange interaction. This interaction is strong because the SE path Cu−Cl_s−Cu consists of two short Cu−Cl_s bonds and because the ∠Cu−Cl_s−Cu bond angle (107.9°) deviates substantially from 90°. The SE interaction J_2 is negligible because the magnetic orbital planes of the two spin sites are nearly orthogonal to each other so that the overlap between the magnetic orbitals is small. The SSE interaction J_3 is substantial ($J_3/J_1 = 0.47$) because the ∠Cu−Cl···Cl angle (159.2°) is not far from 180° so that the magnetic orbitals of the two spin sites overlap well. In essence, the spin lattice of the distorted $CuClO_2$ layer is defined by the two spin exchange interactions, J_1 and J_3. As depicted in Figure 7, this two-dimensional (2D) spin lattice consists of strongly interacting uniform chains.

For the $CuClO_2$ layer composed of 2*n*-ring clusters depicted in Figure 4a, Table 1 shows that the SE interaction J'_1 is negligible because the magnetic orbital planes of the two spin sites are essentially parallel to each other. The strongest antiferromagnetic spin exchange interaction is the intracluster interaction J'_3, which is stronger than either the intercluster interaction J'_2 or the intracluster interaction J'_4 by a factor of approximately two. In short, the spin lattice associated with the interactions J'_1−J'_4 cannot give rise to

(10) Clementi, E.; Roetti, C. *At. Data Nucl. Data Tables* **1974**, *14*, 177.
(11) Our calculations were carried out by employing the SAMOA (Structure and Molecular Orbital Analyzer) program package (Dai, D.; Ren, J.; Liang, W.; Whangbo, M.-H. http://chvamw.chem.ncsu.edu/, 2002).

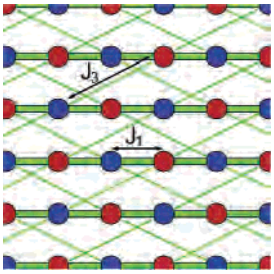

Figure 7. Spin lattice for the distorted $CuClO_2$ layer defined by the two spin exchange interactions J_1 and J_3, where $J_3/J_1 = 0.47$.

simple uniform spin lattices such as uniform chains and 2D square/rectangular lattices.

As far as the disorder of the Cl-atom position is concerned, each $CuClO_2$ layer can be regarded as composed of $CuClO_2$ chains (Figure 3) or as composed of various 2*n*-ring clusters with or without long-range order (Figure 4). It is important to examine whether the spin lattices associated with such $CuClO_2$ layers can give rise to a spin gap. This question is probed in the next section.

3. Predicting a Spin Gap on the Basis of the Classical Spin Approximation

3.1. Quantum Versus Classical Spin Descriptions of Energy Spectrum. Suppose that a magnetic system of M spin sites with spin s_μ at each spin site μ (=1, 2, ..., M) is described by a spin Hamiltonian $\hat{H}$. In principle, the energy spectrum of this system can be determined by evaluating the matrix representation of $\hat{H}$ in terms of a set of basis functions and then diagonalizing the resulting matrix. For simplicity, assume that all the spin sites have a same magnetic ion so that $s_1 = s_2 = ... = s_M = s$. Then, each spin site μ is represented by $2s + 1$ spin basis functions $|s, m_s\rangle_\mu$ ($m_s = -s, -s + 1, ..., s - 1, s$), and the basis functions for the system by the product functions,

$$|s, m_s\rangle_1 |s, m_s\rangle_2 ... |s, m_s\rangle_M$$

The total number of such spin basis functions is $(2s + 1)^M$, and the eigenstates of the system are constructed as linear combinations of these functions, so that the matrix representation of $\hat{H}$ becomes a $(2s + 1)^M \times (2s + 1)^M$ matrix. With increasing M, the number $(2s + 1)^M$ quickly becomes large, thereby making it impossible to determine the eigenvalue spectrum on the basis of diagonalizing the matrix representation of $\hat{H}$.[12] Thus, it is a difficult and challenging task to determine the eigenvalue spectra of extended spin lattices.[8,13−16]

In the classical spin approximation,[9b,17] each spin site is represented by a spin moment σ_μ^0 ($\mu = 1, 2, ..., M$) under the assumption that it can adopt all possible orientations in space rather than the $2s + 1$ directions allowed in quantum mechanics. The energy states of a magnetic system are then determined as linear combinations of the M basis functions σ_μ^0 ($\mu = 1, 2, ..., M$). This way of generating a magnetic energy spectrum is analogous in spirit to that of estimating an electronic energy spectrum by solving an eigenvalue equation with an effective one-electron Hamiltonian (e.g., a Fock equation in Hartree−Fock theory and the equivalent Kohn−Sham equation in density functional theory).[18] The magnetic energy spectrum obtained from the classical spin approximation does not include many-body electron correlation effects. Nevertheless, given that a rigorous theoretical analysis [8,13,14,16] cannot readily address the question of whether a 2D spin lattice with a large unit cell size (e.g., that shown in Figure 7, see below) has a spin gap, it is desirable to be able to provide a plausible answer to such a question. For this purpose, we examine in the next section whether the occurrence of a spin gap in a spin lattice can be related to the energy spectrum of the lattice obtained by the classical spin approximation.

3.2. Eigenvalue Spectra of Simple Spin Lattices. The total spin exchange energy of an ordered spin arrangement of a magnetic system can be estimated by using the Freiser method,[9b,17] which assumes that spins adopt all possible directions in space (i.e., the classical spin approximation) and the spin exchange interactions are isotropic (i.e., a Heisenberg description). In a long-range ordered magnetic state of a magnetic system, the spin sites μ (=1, 2, ..., m) of its unit cell located at the coordinate origin (i.e., the lattice vector $\mathbf{R} = 0$) have the spin moments σ_μ^0. For a magnetic solid with repeat vectors **a**, **b**, and **c**, the ordered spin arrangement is described by the spin functions $\sigma_\mu(\mathbf{k})$,

$$\sigma_\mu(\mathbf{k}) = \frac{1}{\sqrt{M}} \sum_{\mathbf{R}} \sigma_\mu^0 \exp(i\mathbf{k}\cdot\mathbf{R}) \qquad (2)$$

where M is the number of unit cells in the magnetic solid, **k** is the wave vector, and **R** is the direct lattice vector.[19] The ordered magnetic state $\psi_i(\mathbf{k})$ ($i = 1 - m$) is then expressed as a linear combination of the spin functions $\sigma_\mu(\mathbf{k})$,

$$\psi_i(\mathbf{k}) = C_{1i}(\mathbf{k})\sigma_1(\mathbf{k}) + C_{2i}(\mathbf{k})\sigma_2(\mathbf{k}) + ... + C_{mi}(\mathbf{k})\sigma_m(\mathbf{k}) \qquad (3)$$

To determine the energy $E_i(\mathbf{k})$ of the state $\psi_i(\mathbf{k})$ and the coefficients $C_\mu i(\mathbf{k})$ ($\mu = 1 - m$), one needs to evaluate the spin exchange interaction energies $\xi_{\mu\nu}(\mathbf{k})$ between every two spin functions $\sigma_\mu(\mathbf{k})$ and $\sigma_\nu(\mathbf{k})$,

$$\xi_{\mu\nu}(\mathbf{k}) = -\sum_{\mathbf{R}} J_{\mu\nu}(\mathbf{R}) \exp(i\mathbf{k}\cdot\mathbf{R}), \qquad (4)$$

(12) Dai, D.; Whangbo, M.-H. *J. Chem. Phys.* **2004**, *121*, 672.
(13) Barnes, T. *Int. J. Mod. Phys. C* **1991**, *2*, 659.
(14) Dagotto, E. *Rev. Mod. Phys.* **1994**, *66*, 763.
(15) Johnston, D. C.; Kremer, R. K.; Troyer, M.; Wang, X.; Klumper, A.; Bud'ko, S. L.; Panchula, A. F.; Canfield, P. C. *Phys. Rev. B* **2000**, *61*, 9558.
(16) *Quantum Magnetism* (*Lecture Notes in Physics, Vol. 645*); Schollwöck, U., Richter, J., Farnell, D. J. J., Bishop, R. F., Eds.; Springer: New York, 2004.
(17) Freiser, M. J. *Phys. Rev.* **1961**, *123*, 2003.
(18) Wimmer, E. In *Density Functional Methods in Chemistry*; Labanowski, J. K., Andzelm, J. W., Eds.; Springer-Verlag: New York, 1991; Ch. 2.
(19) Given the lattice vector written as $\mathbf{R} = n_a\mathbf{a} + n_b\mathbf{b} + n_c\mathbf{c}$, where n_a, n_b, and n_c are integers, and the wave vector **k** written as $\mathbf{k} = x_a\mathbf{a}^* + x_b\mathbf{b}^* + x_c\mathbf{c}^*$, where $\mathbf{a}^*$, $\mathbf{b}^*$, and $\mathbf{c}^*$ are the reciprocal vectors, and x_a, x_b, and x_c are dimensionless numbers, the $\exp(i\mathbf{k}\cdot\mathbf{R})$ term becomes $\exp[i2\pi(x_a n_a + x_b n_b + x_c n_c)]$.

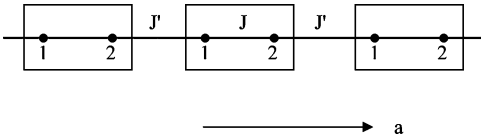

Figure 8. 1D chain lattice made up of spin dimers with repeat distance as described by two spin exchange parameters J and J'.

and diagonalize the resulting interaction matrix $\Xi(\mathbf{k})$,

$$\Xi(\mathbf{k}) = \begin{pmatrix} \xi_{11}(\mathbf{k}) & \xi_{12}(\mathbf{k}) & ... & \xi_{1m}(\mathbf{k}) \\ \xi_{21}(\mathbf{k}) & \xi_{22}(\mathbf{k}) & ... & \xi_{2m}(\mathbf{k}) \\ ... & ... & ... & ... \\ \xi_{m1}(\mathrm{k}) & \xi_{m2}(\mathbf{k}) & ... & \xi_{mm}(\mathbf{k}) \end{pmatrix} \quad (5)$$

This method of calculating the total spin exchange interaction energy was originally developed to predict the superstructure of a magnetic system by finding the wave vector at which its global energy minimum occurs.[9b,17]

It is noted that a spin gap does not occur for an antiferromagnetic uniform chain of spin-1/2 ions, but it does for an isolated spin dimer of spin-1/2 ions and for an antiferromagnetic alternating chain of spin-1/2 ions.[15,20,21] To examine if these observations can be related to the energy spectra of these systems determined by the Freiser method, we consider a chain made up of spin dimers with repeat distance a, which is described by two spin exchange parameters J and J' (Figure 8). This system represents a collection of isolated antiferromagnetically coupled dimers if $J < 0$ and $J'/J = 0$, an antiferromagnetically coupled alternating chain if $J < 0$ and $0 < J'/J < 1$, and an antiferromagnetically coupled uniform chain if $J < 0$ and $J'/J = 1$. For this one-dimensional (1D) system, $\mathbf{k} = x_a(2\pi/a)$ where x_a is a dimensionless number.[19] Each unit cell of this chain has two spin sites so that there are two spin basis functions $\sigma_1(\mathbf{k})$ and $\sigma_2(\mathbf{k})$. The nonzero energy matrix elements $\xi_{\mu\nu}(\mathbf{k})$ (μ, $\nu = 1, 2$) are given by

$$\xi_{12}(\mathbf{k}) = \xi_{21}(\mathbf{k}) = -J - J' \cos(2\pi x_a) \quad (6)$$

which lead to the two energy bands

$$E_1(\mathbf{k}) = +J + J' \cos(2\pi x_a)$$

$$E_2(\mathbf{k}) = -J - J' \cos(2\pi x_a) \quad (7)$$

Plots of $E_1(\mathbf{k})$ and $E_2(\mathbf{k})$ as a function of $\mathbf{k}$ are presented in Figure 9. For $J'/J = 0$ (Figure 9a), the two bands are flat since the interaction between adjacent dimers is zero. The lower band represents the fact that each dimer is in the ground singlet state, and the upper band that each dimer is in the excited triplet state. The presence of an energy gap between the two bands is consistent with the fact that each isolated spin dimer has a spin gap. For $0 < J'/J < 1$ (Figure 9b), the two bands are separated by an energy gap. The top of the lower band represents the state in which each dimer in the ground singlet state interacts ferromagnetically with its nearest-neighbor dimers (Figure 10a), and the bottom of the upper band the state in which each dimer in the excited triplet state interacts antiferromagnetically with its nearest-neighbor dimers (Figure 10b). As long as $0 < J'/J < 1$, these two states differ in energy so that the two bands are separated by an energy gap. This is consistent with the fact that an antiferromagnetic alternating chain has a spin gap. For $J'/J = 1$ (Figure 9c), the two bands merge because the top of the lower band becomes the same in energy as the bottom of the upper band, so that there is no energy gap between the two bands. This is consistent with the fact that an antiferromagnetic uniform chain does not have a spin gap. Obviously, use of this classical spin approach is not appropriate for a Haldane system (i.e., a uniform chain made up of integer-spin ions), which has a spin gap due to a many-body electron correlation.[20,22]

As another example, we examine the 2D spin lattice in which dimers repeat along the two orthogonal directions with

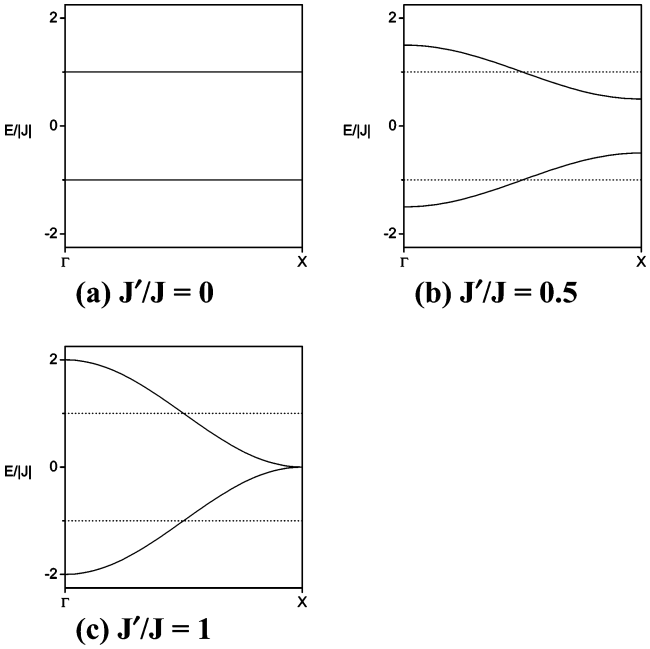

Figure 9. Dispersion relations of the two spin bands associated with the 1D chain lattice of Figure 8 for the cases of (a) $J'/J = 0$, (b) $J'/J = 0.5$, and (c) $J'/J = 1$.

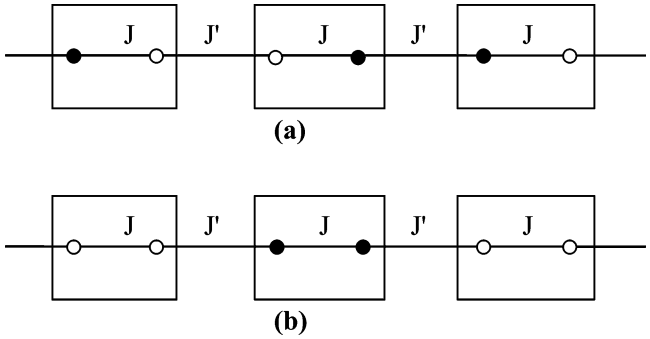

Figure 10. Spin arrangements of the 1D chain lattice of Figure 8 at (a) the top of the lower-lying spin band and (b) the bottom of the higher-lying spin band. The filled and unfilled circles represent the up-spin and down-spin, respectively.

(20) Kahn, O. *Molecular Magnetism*: VCH: New York, 1993.
(21) Mikeska, H.-J.; Kolezhuk, A. K. In *Quantum Magnetism* (*Lecture Notes in Physics, Vol. 645*); Schollwöck, U., Richter, J., Farnell, D. J. J., Bishop, R. F., Eds.; Springer: New York, 2004; Chapter 1.
(22) Haldane, F. D. M. *Phys. Rev. Lett.* **1983**, *50*, 1153.

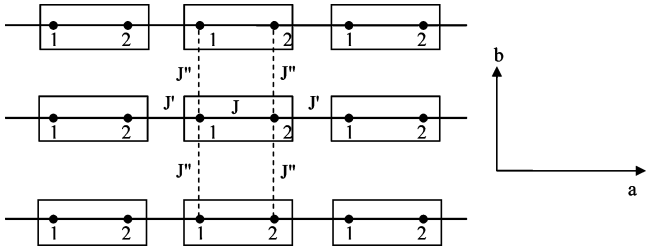

Figure 11. 2D spin lattice made up of spin dimers with repeat distances a and b described by two spin exchange parameters J and J'.

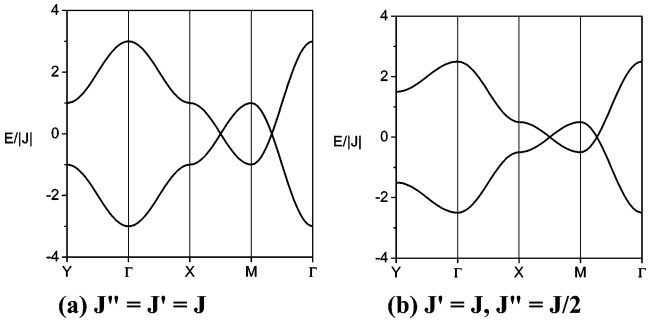

Figure 12. Dispersion relations of the two spin bands associated with the 2D lattice of Figure 11 for the cases of (a) $J'' = J' = J$ and (b) $J'' = J/2$ and $J' = J$.

repeat distances a and b (Figure 11). This 2D spin lattice is described by three spin exchange parameters J, J', and J'' with two basis functions, $\sigma_1(\mathbf{k})$ and $\sigma_2(\mathbf{k})$. It becomes a rectangular spin lattice when $J = J'$ and $0 < J''/J < 1$, and a square spin lattice when $J = J' = J''$. The nonzero energy matrix elements, $\xi_{\mu\nu}(\mathbf{k})$, are given by

$$\xi_{12}(\mathbf{k}) = \xi_{21}(\mathbf{k}) = -J - J'\cos(2\pi x_a) - 2J''\cos(2\pi x_b) \quad (8)$$

which lead to the two energy bands

$$E_1(\mathbf{k}) = +J + J'\cos(2\pi x_a) + 2J''\cos(2\pi x_b)$$

$$E_2(\mathbf{k}) = -J - J'\cos(2\pi x_a) - 2J''\cos(2\pi x_b) \quad (9)$$

Plots of $E_1(\mathbf{k})$ and $E_2(\mathbf{k})$ as a function of $\mathbf{k}$ are presented in Figure 12a for a square lattice and in Figure 12b for a rectangular lattice. In both cases, the lower band is not separated from the upper band, so the classical spin analysis predicts that both lattices do not have a spin gap. This prediction is consistent with the finding that a square spin lattice made up of spin-1/2 ions has no spin gap.[7,8,23]

The above discussion suggests that the classical spin approximation can provide a plausible answer to the question whether a spin lattice has a spin gap. This simple approach would fail for a magnetic system whose eigenvalue spectrum depends strongly on many-body electron correlation effects. Consider a spin ladder made up of spin-1/2 ions that is described by the spin exchange J along the leg and the spin exchange $J_\perp$ along the rung ($J_\perp/J > 0$). When the interchain interaction is very weak ($J_\perp \ll J$), the ladder consists of very weakly interacting uniform chains. When calculated using the classical spin approximation, the energy spectrum of such a ladder shows no spin gap (not shown). However, numerical solutions for the eigenvalue spectrum of a spin ladder made up of spin-1/2 ions on the basis of a rigorous theoretical method [24] showed that it has a spin gap even when $J_\perp \ll J$ as long as $J_\perp$ is nonzero. In a sense, a spin ladder consisting of two weakly interacting uniform chains of spin-1/2 ions behaves as a Haldane system, i.e., a single uniform chain made up of spin-1 ions.

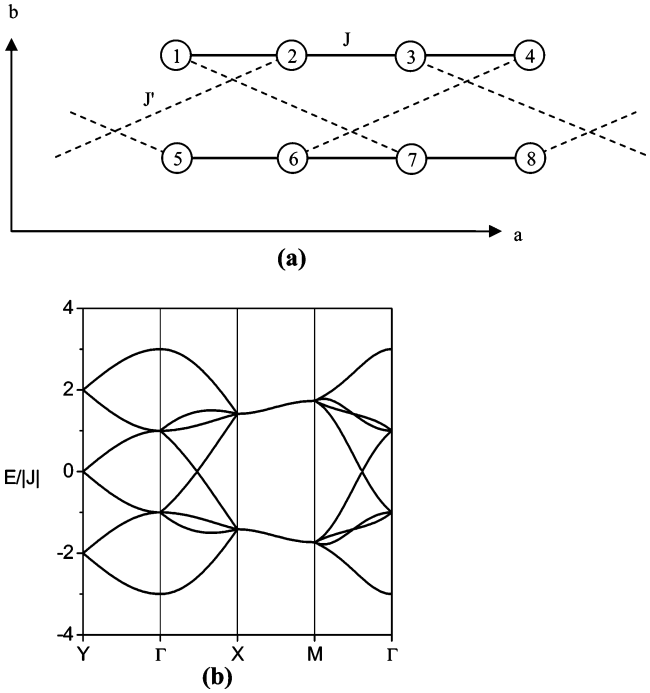

Figure 13. (a) 2D spin lattice of Figure 7 that is made up of eight spin sites per unit cell with repeat distances a and b and that is described by two spin exchange parameters J and J'. (b) Dispersion relations of the eight spin bands associated with the 2D chain lattice of Figure 13a, where $J'/J = 0.5$.

Table 3. Nonzero Energy Matrix Elements $\xi_{\mu\nu}(\mathbf{k})$ (μ, $\nu = 1-8$) Associated with the Basis Functions $\sigma_\mu(\mathbf{k})$ ($\mu = 1-8$)

$\xi_{12}(\mathbf{k}) = \xi_{23}(\mathbf{k}) = \xi_{34}(\mathbf{k}) = \xi_{56}(\mathbf{k}) = \xi_{67}(\mathbf{k}) = \xi_{78}(\mathbf{k}) = -J$
$\xi_{14}(\mathbf{k}) = \xi_{58}(\mathbf{k}) = -J\exp(i2\pi x_a)$
$\xi_{17}(\mathbf{k}) = -J' - J'\exp[-i2\pi(x_a + x_b)]$
$\xi_{46}(\mathbf{k}) = -J' - J'\exp[-i2\pi(x_a - x_b)]$
$\xi_{28}(\mathbf{k}) = -J'\exp(-i2\pi x_a) - J'\exp(-i2\pi x_b)$
$\xi_{35}(\mathbf{k}) = -J'\exp(i2\pi x_a) - J'\exp(-i2\pi x_b)$

3.3. Spin Lattice of the CuClO$_2$ Layer. The 2D spin lattice of Figure 7 consists of interacting uniform chains and is effectively a 2D rectangular lattice. Consequently, this spin lattice is not expected to have a spin gap. A unit cell of the spin lattice of Figure 7 has eight spin sites and hence eight basis functions $\sigma_\mu(\mathbf{k})$ ($\mu = 1-8$) (Figure 13a), and this lattice is formed by two exchange parameters (here designated as J and J'). The nonzero energy matrix elements $\xi_{\mu\nu}(\mathbf{k})$ (μ, $\nu = 1-8$) associated with these basis functions are summarized in Table 3. The eight energy bands $E_\mu(\mathbf{k})$ ($\mu = 1-8$) resulting from these spin exchange interactions are plotted as a function of $\mathbf{k}$ in Figure 13b, which shows that all the bands overlap. Thus, as expected, it is unlikely that the 2D spin

(23) Richter, J.; Schulenburg, J.; Honecker, A. In *Quantum Magnetism* (*Lecture Notes in Physics, Vol. 645*); Schollwöck, U., Richter, J., Farnell, D. J. J., Bishop, R. F., Eds.; Springer: New York, 2004; Chapter 2.

(24) Barnes, T.; Dagotto, E.; Riera, J.; Swanson, E. S. *Phys. Rev. B* **1993**, *47*, 3196.

lattice of interacting chains (Figure 7) has a spin gap. This in turn means that this 2D spin lattice cannot be a correct model for interpreting the magnetic properties of (CuCl)-$LaNb_2O_7$.

Thus, we are compelled to ask what kind of spin lattice is required for each $CuClO_2$ layer to have a spin gap. In a $CuClO_2$ layer composed of 2*n*-ring clusters of different sizes (e.g., Figure 4), the intra- and intercluster spin exchange interactions cannot lead to simple uniform spin lattices such as uniform chains and 2D square/rectangular spin lattices. As a consequence, the magnetic energy levels of such a $CuClO_2$ layer are better described by discrete energy levels (associated with the constituent ring clusters) rather than by magnetic energy bands and hence should exhibit a spin gapped behavior. In other words, the disorder of the Cl-atom position in (CuCl)$LaNb_2O_7$ and the spin gapped behavior of (CuCl)$LaNb_2O_7$ are accounted for if the $CuClO_2$ layers have $CuCl_4O_2$ octahedra with both linear and nonlinear $Cl_s-Cu-Cl_s$ units such that the $CuClO_2$ layers consist of 2*n*-ring clusters of varying sizes with no long-range order. As will be discussed in the next section, however, this picture needs a slight modification to accommodate results of the recent neutron scattering[4] and magnetization[5] studies on (CuCl)-$LaNb_2O_7$.

4. Discussion

From their neutron neutron scattering experiments[4] Kageyama et al. found that the magnetic excitations of (CuCl)-$LaNb_2O_7$ exhibit no strong two-dimensionality as if the $CuClO_2$ layers consist of weakly interacting clusters that are coupled antiferromagnetically. Such magnetic clusters can be identified as 2*n*-ring clusters. The neutron scattering experiments show a sharp peak at 2.3 meV, which corresponds to the spin gap found from the magnetic susceptibility measurements at 0.1 T (i.e., $\Delta = 2.3$ meV $= 26.7$ K).[4] This finding implies that there is a narrow range of preferred size for the 2*n*-ring clusters because the spin gap of a 2*n*-ring cluster should decrease with increasing *n*. The neutron scattering study also shows a small peak at 5.0 meV whose temperature dependence is similar to that of the 2.3 meV peak. The origin of the 5.0 meV peak is not well understood, although the collective bound state excitation of several elementary triplets has been considered as a possible origin.[4] It is tempting to suggest that the 5.0 meV excitation is a spin gap of small 2*n*-ring clusters.

The magnetization study of (CuCl)$LaNb_2O_7$ by Kageyama et al.[5] presents a more complex spin gapped behavior: (a) the spin gap disappears at 10.3 T, which is much lower than expected from the spin gap, i.e., 18.4 T ($= \Delta/g\mu_B$), and (b) the magnetization increases linearly without any trace of fractional plateaus until it saturates at 30.1 T. According to observation (a), the apparent spin gap determined from the magnetization experiments is considerably smaller than that deduced from the magnetic susceptibility and neutron scattering experiments. Observation (b) implies that interactions among magnetic excitations are substantial, as typically found for a one-dimensional magnet, which is in apparent contradiction to the localized nature of the triplet excitations found from the neutron scattering experiments.[4] As to why (a) and (b) are observed in the magnetization experiments, Kageyama et al.[5] have considered a number of possible scenarios. The investigation of this question is beyond the scope of the present work. Nevertheless, one may speculate if the observation (b) has a structural origin. For example, suppose that the 2*n*-ring clusters responsible for the 2.3 meV gap are large enough that their two constituent chain fragments of *n* spin sites may behave like extended chains. Then, the localized nature of the triplet excitations may reflect weak interactions between adjacent 2*n*-ring clusters, while the sizable interactions among magnetic excitations detected by the magnetization study may reflect interactions within each 2*n*-ring cluster. If this reasoning is correct, the observation (a) should originate from the property of a 2*n*-ring cluster. A plausible scenario would be that a 2*n*-ring cluster has a bound state with $S = 2$, which is one of the several scenarios suggested by Kageyama et al.[5]

5. Concluding Remarks

A 2D square spin lattice is not a proper model for describing the magnetic properties of (CuCl)$LaNb_2O_7$ due to the disorder of its Cl-atom position. This disorder indicates that the Cu^{2+} ions of the $CuCl_4O_2$ octahedra have the four-short-two-long coordinate environments, and such $CuCl_4O_2$ octahedra appear in the $CuClO_2$ layers without long-range order in their orientation and shape. If the $Cl_s-Cu-Cl_s$ units of the $CuCl_4O_2$ octahedra are restricted to be linear, each $CuClO_2$ layer is divided into $CuClO_2$ chains, thereby leading to a 2D spin lattice of strongly interacting uniform chains. The classical spin analysis suggests that this 2D spin lattice does not have a spin gap and hence cannot explain the presence of a spin gap in (CuCl)$LaNb_2O_7$. For each $CuClO_2$ layer to have a spin gap, it should have $CuCl_4O_2$ octahedra with both linear and nonlinear $Cl_s-Cu-Cl_s$ units such that there occur no uniform chains but 2*n*-ring clusters of certain size with no long-range order. This structural model of magnetic clusters should be taken into consideration in interpreting the magnetic properties of (CuCl)$LaNb_2O_7$ determined by neutron scattering and magnetization experiments.

It is intriguing that the general features of the magnetic susceptibility of (CuCl)$LaNb_2O_7$ are reasonably well approximated by an isolated spin dimer model with the Cu··Cu distance found for the fourth nearest-neighbor spin exchange interaction J_c (Figure 1d). In the fitting analysis of the neutron scattering intensity profile using an isolated spin dimer model,[4] it is implicitly assumed that the orientation of an isolated spin dimer is random and is independent of those of other isolated spin dimers. This assumption is valid when each crystallite of a powder sample contains only one isolated spin dimer. The latter is highly unlikely so that the intriguing observation is most likely a fortuitous one.

Acknowledgment. The research was supported by the Office of Basic Energy Sciences, Division of Materials Sciences, U. S. Department of Energy, under Grant No. DE-FG02-86ER45259. We thank Dr. Reinhard K. Kremer and Dr. Andreas Voigt for invaluable discussion and references.

IC060104W